CORRECTION OF THE RESPIRATORY MOTION OF THE HEART FROM 4D MYOCARDIAL IMAGES

By

JING SUN

A THESIS PRESENTED TO THE GRADUATE SCHOOL
OF THE UNIVERSITY OF FLORIDA IN PARTIAL FULFILLMENT
OF THE REQUIREMENTS FOR THE DEGREE OF
MASTER OF SCIENCE

UNIVERSITY OF FLORIDA

2006

Dedicated to my beloved parents and my husband

谨以此文献给我深爱的父亲母亲和丈夫

ACKNOWLEDGMENTS

First of all, I would like to express my deep indebtedness and my sincere gratitude to my advisor, David Gilland, for the valuable guidance, support and continuous encouragement he has given me during the course of this work. His insight in this field and his thoughtful personality have made my study here worthwhile and unforgotten. I am also equally indebted to the members of my committee, Wesley Bolch and David Hintenlang, for their helpful advice, suggestions and encouragements. Special thanks are also extended to Bernard Mair, the external committee member, for his suggestions and attendance. It is a great honor to have them on my committee.

I am grateful to Willams Paul Segars, for his tremendous help with the NCAT phantom. I would like to thank Dr. Zixiong Cao for his patience and help to set up this research idea. I am also grateful to Uday Tipnis, Keelan Seabolts, and Jason Parker, who have inspired and assisted in my research study.

Finally I would like to extend my sincere gratitude to my parents for their moral support from far away in my home country, China. I would like to thank my husband Dapeng for his love, understanding and moral support.

TABLE OF CONTENTS

page

LIST OF TABLES

LIST OF FIGURES

Abstract of Thesis Presented to the Graduate School
of the University of Florida in Partial Fulfillment of the
Requirements for the Degree of Master of Science

CORRECTION OF THE RESPIRATORY MOTION OF THE HEART
FROM 4D MYOCARDIAL IMAGES

By

Jing Sun

August 2006

Chair: David Gilland
Major Department: Nuclear and Radiological Engineering

During myocardial nuclear medicine imaging, respiratory motion blurs the projection data and thus causes diagnostic artifacts. A method is developed and evaluated in this work to compensate for effects of respiratory motion in four dimensional (4D) gated cardiac Emission Computed Tomography (ECT). Non-uniform-rational-B-splines-based CArdiac Torso (NCAT) phantoms were generated to simulate temporal frames regularly spaced during combined respiratory and beating heart cycles. Projection data were acquired at 60 positions over 180 degrees to model gated myocardial perfusion Single Photon Emission Computed Tomography (SPECT) with Technetium-99m (Tc-99m) sestamibi. A 2-cm respiratory rigid body translation was simulated for the axial heart movement during normal tidal breathing. The motion was tracked and estimated by calculation of the axial center-of-mass (aCOM). Respiratory motion correction was applied to the simulated projection data. The 4D image reconstruction and 3D cardiac wall motion estimation for all temporal frames were

performed simultaneously by a Joint 4D Reconstruction and Motion estimation method (RM). The Sum of Squared Errors (SSE) was calculated to evaluate the image quality, and the Phantom-matching Motion Errors (PME) was computed to evaluate the wall motion estimation accuracy.

After respiratory motion compensation, the image quality, such as spatial resolution, of corrected images was better than that of respiratory blurred images, and very close to the quality of the images obtained when no respiratory motion was present. The accuracy of cardiac wall motion estimates was also improved with respiratory motion compensation.

CHAPTER 1
INTRODUCTION

1.1 An Overview

Respiratory motion takes place during myocardial perfusion imaging and image blurring due to patient respiration is thus unavoidable. This respiratory effect is not negligible; it degrades the diagnostic accuracy when appropriate respiratory motion compensation is absent. Many researchers have offered methods to reduce the impact of respiratory motion on image quality. One of the common methods is to let the patients hold their breath during imaging [1]. The main disadvantage of this method is that the patient needs to be highly cooperative in order to obtain accurate images. Also, in this method, imaging has to be performed repeatedly and during each acquisition, the patient may not hold his/her breathe at the same level as the previous acquisitions, which will still lead to image blurring. Using an external device, for e.g. a sensor, to set up a respiratory gating system is an alternate method to reduce the respiratory motion effect [2-4]. Respiratory motion is not stable or perfectly repeatable like beating heart motion. Therefore, it is difficult to have a system that both measures the respiratory cycle accurately such as electrocardiography (ECG) measurements of the beating heart cycle, and is acceptable to both patients and technologists. Currently, Center-of-Mass is the most popular method used to track and estimate respiratory motion. This method requires only the patient projection data and has been realized in both digital [5, 6] and analogy adjustments of the axial signal [7, 8].

1.2 Literature Review

There are numerous papers published on blurring due to patient motion and correction methods. Recent works have paid more attention on Positron Emission Tomography (PET) and SPECT studies. In 1995, using MRI imaging, Wang *et al.* [9], determined how much the heart shifted due to respiratory motion. It was concluded that during normal tidal breathing the movement of the heart due to respiration is dominated by superior-inferior (SI) motion, which is linearly related to the SI motion of the diaphragm. Some gating systems were developed for SPECT and PET imaging to decrease the respiratory motion artifacts during imaging acquisition, for e.g., Macintosh platform and LabView environment real time system developed by Klein *et al.* [3], and respiratory gated SPECT (RGS) system realized by Cho [10]. Segars *et al.* [11, 12] have performed simulation studies to study respiratory motion effects on myocardial SPECT with the spline-based Mathematical Cardiac Torso (MCAT) phantoms. Respiratory mechanics were modeled in MCAT phantoms for SPECT imaging, and this work led to the improved and more realistic 4D NCAT phantom. Feng *et al.* [13] and Bruyant *et al.* [14] have developed several methods to compensate for effects of respiratory motion by applying center-of-mass algorithms to reconstructed images or projection datasets. They implemented their method with simulated MCAT phantoms. However, their work focused on respiratory motion only and the heart wall was assumed to be stationary in their SPECT myocardial perfusion study.

1.3 Our Method

The goal of this study is to develop a motion compensation method using center-of-mass algorithm to apply to 4D SPECT projection data simulated with both beating heart motion and respiratory motion. We implement this method to improve the reconstructed

image quality and cardiac wall motion estimation accuracy, for the images reconstructed and motions estimated simultaneously by RM algorithm.

CHAPTER 2
RESPIRATORY MOTION COMPENSATION, IMAGE RECONSTRUCTION, AND CARDIAC WALL MOTION ESTIMATION METHODS

2.1 Introduction

To compensate respiratory motion effects, Non-uniform-rational-B-splines-based Cardiac Torso (NCAT) phantoms were generated to model the realistic organs in the torso, and simulate the beating heart motion and respiratory motion [15]. The 2D projection data of NCAT phantoms were obtained by the Radon transform. Data acquisition was simulated in SPECT by using a parallel-hole collimator geometry [16]. The respiratory motions were estimated by the axial Center-of-Mass algorithm (aCOM) [14] for the projection data. The motion compensations were also applied to the 4D projections. The image reconstruction and 3D cardiac wall motion estimation for all temporal frames were performed simultaneously by a joint 4D Reconstruction and Motion estimation method (RM) [16]. The image quality before and after compensation was evaluated by calculations of the Sum of Squared Errors (SSE), and the myocardial wall motion estimation accuracy was evaluated by computations of the Phantom-matching Motion Errors (PME) [17].

2.2 NCAT Phantom Simulation

The NCAT phantoms and the cardiac wall motion fields were generated by NCAT C language software developed in John Hopkins University. Motion vectors were calculated and assigned in MATLAB to each voxel in each frame from the NCAT

software outputs. Projection datasets were also computed by using a linear interpolation projector in MATLAB.

2.2.1 Myocardial Phantom Simulation

The NCAT phantom provides a realistic source distribution that models gated myocardial perfusion imaging with Tc-99m sestamibi by using the Non-uniform Rational B-Splines (NURBS) method to define the anatomy of a human body at a series of phases over cardiac cycles and respiratory cycles. This phantom can be used to study the development of image acquisition strategies, image processing and reconstruction algorithms and compensation methods. It can be used to research the effects of anatomical variations and patient motions, such as the beating heart and respiratory motions, on medical images. NCAT phantom simulation software was developed at the Johns Hopkins University and fully described by Segars *et al*. [11, 12].

In this work, a 40 temporal frames NCAT phantom was generated over one entire respiratory cycle with both beating heart motion and respiratory motion by the NCAT software. The first frame corresponded to the full exhalation of the respiratory cycle and the end-diastole of the beating heart cycle. The length of respiratory cycle was set to 5 seconds as a normal tidal breathing. The respiratory cycle started from full exhalation. At 0.455, almost in the middle, of the entire respiratory cycle, motion reached the full inhalation. The length of cardiac cycle was set to 1 second as a normal male heart beating. Therefore, the phantom included one completed respiratory motion cycle and five completed beating heart motion cycles. For each cardiac cycle, there are 8 temporal frames. Frame 1 was the end-diastole, and frame 4 was the end-systole. Due to the respiratory motion, the diaphragm motion and chest Anterior-Posterior (AP) expansion were also simulated. The extent of the maximum diaphragm motion was set to 2

centimeters. This motion was simulated as a translation motion along the body axis. The extent of the maximum chest AP expansion was set to 1.2 centimeters. This motion only effect ribcage, body and lungs. Since heart is the only organ included in the NCAT myocardial phantom, there was no motion along trans-axial direction modeled in this present study. The projection data will show the heart movement due to respiratory motion in chapter 3. For the heart, the length of the left ventricle myocardium was 9.43 centimeters, and the average radius of the left ventricle was 2.97 centimeters. The volume of left ventricle chamber at the end-diastole was 108.36 ml, and at the end-systole was 42.21 ml. So for this simulated NCAT phantom, the stroke volume (the amount of blood pumped by the left ventricle of the heart in one contraction) was 66.15 ml and the ejection fraction (the fraction of blood pumped out of a ventricle with each heart beat) was 61%. For each frame, 50 slices of a male torso in supine position were created. Within each slice, the dimension of the phantom was 96×96. The voxel size was 0.30 centimeters. The phantom provides a realistic source distribution that models gated myocardial perfusion imaging with Tc-99m sestamibi. Activities within myocardial region (including left ventricle myocardium, right ventricle myocardium, left atrium myocardium, and right atrium myocardium) were assigned to 75 source intensity per cm^3 for Tc-99m, energy in 140 keV. For this study, only myocardial source activity was included. Outside activity was 0 everywhere. The parameters determined for beating heart cycle were modeled based on tagged MR images obtained from Johns Hopkins University [15]. And the parameters determined for respiratory cycle were modeled based on the Visible Human Project CT dataset from the National Library of Medicine [15].

In practice, any continuous function is instantaneous. In order to be more realistic, for each time bin, the time interval for each temporal frame, four consecutive frames were created and averaged over the time bin. In this work, the study was concentrated on the myocardial region. Also to smooth the source distribution, for each frame, the 3D cardiac phantom (96 × 96 × 50) was obtained by linearly collapsing the original torso phantom, which is generated by NCAT software directly with dimension of 256 × 256 × 168 voxels for computational efficiency, and was truncated into dimension 96 × 96 × 50, which included myocardial region, for computation efficiency purpose. Slice 15 to slice 64 was considered and chosen as myocardial region in this present study. And in each slice, pixel 17 to pixel 112 on both two dimensions was used as the final myocardial phantom.

As a reference, a phantom with 8 gated frames over 1-second cardiac cycle with only beating heart motion was generated, with the same size 96 × 96 × 50 voxels for each frame. A segmentation file with intensity equals to "1" inside myocardium and intensity "0" outside was also generated as a map, which defined the heart region by setting a threshold along the myocardial boundary.

The source distributed objects were created as noise-free phantoms. Attenuation effects were not considered for all phantoms generated using the NCAT software in this present study.

2.2.2 Cardiac Wall Motion Simulation

Myocardial wall motion can be computed by NCAT software [15]. A 3D motion field between each two successive temporal frames over one complete beating heart cycle was calculated. For each beating heart cycle, one NCAT software motion calculation generated 8 separate output files if the cardiac cycle was gated into 8 frames. Each

output file included starting points and ending points for and only for those non-zero voxels in the first frame, but not for each non-zero voxel in that frame. Furthermore, more than one motion vector might be assigned to the same non-zero voxel. In this case, the last assigned vector would be selected as the motion vector for this voxel when motion field between these two frames was computed from the output file. For each motion vector of a voxel, the starting point in the starting frame was an integer, and the ending point in the next frame was a real number. The norm of a motion vector was calculated as the distance between the starting point and the ending point. The direction of a motion vector was expressed as three components, namely u(r), v(r), and w(r) along axes x, y, and z, respectively, where r = (x,y,z) denoted the voxel coordinates in the spatial domain. Those motion vectors were considered true motions for each voxel from one time bin to another. Output from the software was processed in MATLAB to calculate the norm and the three components for each motion vector of the voxels. When evaluated the motion fields estimated by RM algorithm, those motion vectors were considered as a reference set. Therefore, the NCAT software-calculated motion fields were named *True motion* in this present study.

2.2.3 Projection Simulation

Forward projections were performed at 60 angles over 180 degrees, which starts from patient left hand side, went in front of the patient, and to the patient right hand side. The 2D projection data were computed by using a linear interpolation projector for each slice per angle per frame. Effects of attenuation, scatter, and random were not considered during projection data acquisition.

Clinically, 2000 counts in the myocardial region per frame per projection angle are realistic for gated Tc-99m sestamibi imaging [18]. All projection data were scaled to this

level. Therefore, the maximum voxel intensity was assigned to 0.237. Poisson noise was added to all of the noise-free projection data after scaling.

Four projection datasets were computed in this study. The first dataset was calculated from the 8-frame beating heart motion only phantom in dimension 96 × 50 × 60 × 8. The dataset was named *Object with beating Heart Motion only (OHM)* in this present study. The second dataset was computed from the 40-frame phantom directly, in dimension 96 × 50 × 60 × 40. This projection was calculated as original raw data for respiratory motion compensation, and was named *Object with Respiratory Motion but Uncorrected (ORMU)* in this present study. A third dataset was simulated as imaging with both beating heart motion and respiratory motion, in dimensions of 96 × 50 × 60 × 8. The 40-frame both motions phantom included one complete respiratory cycle and five beating heart cycles at the same time. Five cardiac cycles divided the respiratory cycle into five phases. For example, five phases for each respiratory cycle could be chosen as a respiratory gate schema. In this case, there were 8 temporal frames for each beating heart cycle over one respiratory phase. Each temporal frame in one beating heart cycle was summed over respiratory phases. Then an averaged 8-frame projection dataset was obtained. It was blurred due to the respiratory motion. The dataset was named *Object with Respiratory Motion and Averaged (ORMA)* in this present study. The last dataset was computed from 40-frame both motion phantom, too. The projection dimension was also as 96 × 50 × 60 × 8. Averaging was done for each temporal frame in each beating heart cycle over five respiratory phases, but after applying aCOM respiratory motion compensation method. The dataset was named *Object with Respiratory Motion but*

Corrected (ORMC) in this present study. All three projection datasets in dimension 96 × 50 × 60 × 8 were in the same noise level.

2.3 Axial Center-of-Mass Motion (aCOM) Estimation and Respiratory Motion Compensation Method

The Center-of-Mass (COM) of each projection data per temporal frame was estimated in MATLAB. By calculating the COM of the integrated projection data per respiratory phase simulated from *ORMU*, the movement due to respiratory motion alone body axis can be determined. To compensate for respiratory effects, each frame was shifted respectively depending on the movement in each respiratory phase to reduce the blurring in each beating heart gate.

2.3.1 Axial Center-of-Mass (aCOM) Calculation

According to Feng *et al*. [13], the COM of each frame had the same rigid-body motion as the object in that frame. The phantom was simulated a 2-centimeter translation motion along the body axis. From full exhalation to full inhalation, the heart moved down linearly with diaphragm up to 2 centimeters. The reference linear translation curve was given by NCAT software, and is shown in Figure 2-1. Example motion curve was given for 20 respiratory phases. COM of projection data computed from *ORMU* for each frame was calculated to track and estimate respiratory motion. To reduce the noise, the projection dataset had been integrated over the trans-axial direction per projection angle, over all of the projection angles, over each beating heart cycle, and over each respiratory phase. The center of mass along the body axis was determined for any respiratory phase as given by formula Equation (2-1):

$$aCOM(f) = \frac{\sum_{j=1}^{K} j \sum_{\theta=1}^{N} \sum_{t=1}^{T} \sum_{i=1}^{M} p(i, j, \theta, t, f)}{\sum_{j=1}^{K} \sum_{\theta=1}^{N} \sum_{t=1}^{T} \sum_{i=1}^{M} p(i, j, \theta, t, f)} \quad , \qquad (2\text{-}1)$$

where M was the total number of voxels in the trans-axial dimension, N was total number of projection angles, T was total number of beating heart gates, K was the total number of voxels in axial dimension, and p (i, j, θ, t, f) was the activity in pixel (i, j) in the projection acquired at angle θ for beating heart time frame t in respiratory phase f.

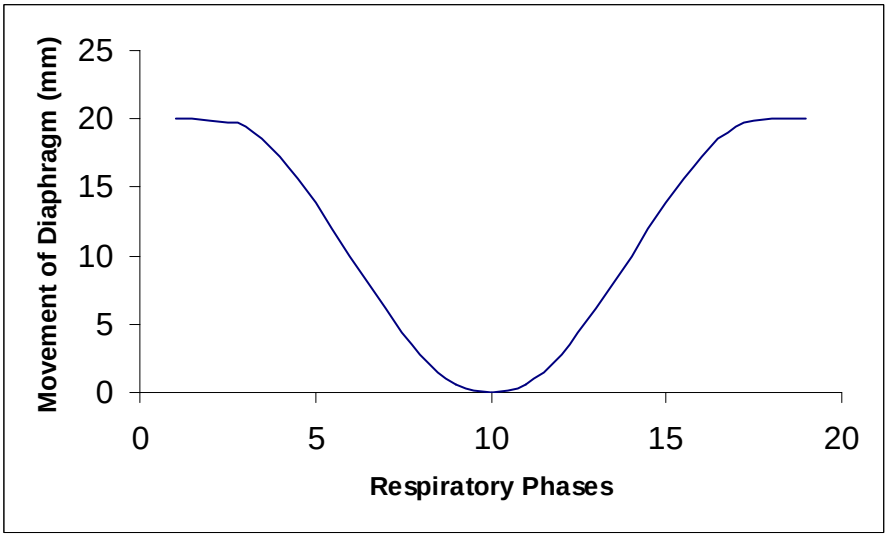

Figure 2-1. Reference linear translation curve was given by NCAT software

Assume within each respiratory phase, that the respiratory motion was constant. Therefore, five aCOM were calculated finally for five phases over one complete respiratory cycle. Each one indicated the axial shift magnitude for the beating heart temporal frames within that respiratory phase. The estimated relative center of mass for each respiratory phase was in unit number of voxels. The voxel size of projection data was 0.3 centimeters.

2.3.2 Respiratory Motion Compensation

Use equation (2-1) to calculate the COM of the projection dataset for each beating heart frame. COMs of 40 temporal frames in total were computed for the five cardiac cycles, as well one entire respiratory cycle.

For motion compensation, each frame of projection dataset *ORMU* was vertically shifted because only axial movement was considered in this study. Full exhalation in the respiratory cycle and end-diastole in the beating heart cycle was defined as the reference status with zero relative movement in this work. Therefore, the last respiratory phase was chosen as the reference phase, for which the projection data were not shifted. All other projections were shifted up. Based on the assumption that respiratory motion was constant within each respiratory phase, the beating heart frame within each respiratory phase will shift same amount. And the magnitude of the shifting was depended on the movement calculated by Equation (2-1) of the phase which the beating heart frame was located. Because the axial shift magnitude was not an integer number of voxels, a linear interpolation was performed along the body axis to obtain an accurate shifting.

After respiratory motion compensation, the COM of each shifted beating heart frames were closed to the COM of the reference phase. The magnitude of the errors depended on how many respiratory phases were chosen. Because, in practice, there are no very accurate devices such as ECG monitors used for cardiac gated imaging, the narrow respiratory gates could not be obtained. Five respiratory phases were chosen because of the simplicity, so that each respiratory phase was reasonably assigned as 1 second. Ten phases and twenty phases respiratory schema were also simulated for optimization and comparison. The aCOM method was also applied to the corrected

projection dataset to check the constancy of the aCOM position during the respiratory cycle. The completed results are listed and shown in Chapter 3.

Conclusively, the motion compensation algorithm can be described as following steps:

1. Calculate the center-of-mass of each respiratory phase.
2. Choose the respiratory phase which has least movement (the phase has smallest center-of-mass value) as the reference phase, and calculate the movements of all other phases by giving relative to the reference phase.
3. Shift all beating heart frames in each respiratory phase axially according to the relative movement calculated for that phase.
4. Sum each beating heart frame over all of the respiratory phases.

2.4 Image Reconstruction and Cardiac Wall Motion Estimation (RM) Method

Projections simulated from *OHM*, *ORMA* and *ORMC* were all reconstructed by image reconstruction and cardiac wall motion estimation (RM) algorithm. This algorithm was first discussed by Mair *et al.* [19] and developed in MATLAB code by Cao *et al.* [20]. The method was later improved and implemented in Fortran code by Gilland *et al.* [21] and Mair *et al.* [17].

2.4.1 RM Algorithm

RM algorithm was a method for gated cardiac ECT that reconstructed the voxel intensities of the gated images and estimated the 3 dimensional motion of the cardiac wall for all frames simultaneously. The algorithm consisted of two steps, the image reconstruction step (R step) and the cardiac wall motion estimation step (M step). It was based on an iterative algorithm for minimizing an objective function that included the negative log likelihood of the data, the standard optical brightness constraint, and a biomechanical model for elastic deformations of the myocardium.

In the early version, Mair *et al.* [19] discussed the estimation of motion and images for only two frames with maximum deformation, end-diastole and end-systole. During R step, the motions were fixed and the objective function was minimized over the frames iteratively. During M step, the frames were fixed and the objective function was minimized over the motion field iteratively based on solving the Euler–Lagrange equations [22, 23]. The algorithm was implemented in MATLAB because of its extensive library of mathematical functions. However, it was rewritten in Fortran language by Gilland *et al.* [21] to enhance the computational efficiency. And the most important point was that, in Mair *et al.* [17] the algorithm was extended from two frames to a complete cardiac cycle frames, which can be any finite number. Eight frames were chosen in this simulation study. Instead of being performed in pairs of frames, a mathematical framework, which included the entire cycle of images and motion fields, was developed to make only one single objective function. In this manner, all frames were considered as a loop. Each update of a frame involved the current estimate of the frame immediately before and after this frame. The objective function minimization was performed directly by using a type of sequential quadratic programming with the conjugate gradient algorithm [17] applied at each step. After all of the improvements and optimizations, the algorithm guaranteed non-negativity of the reconstructed images, and each iteration decreased the value of the objective function. The simultaneous estimation allowed the data to influence both image reconstruction and cardiac wall motion estimation at the same time [17].

2.4.2 Objective Function

In this study, the myocardium was considered as a deformable elastic material satisfying the standard constitutive relations in continuum mechanics [24, 25].

2.4.2.1 Negative log likelihood term

It was assumed that the small deformation between two successive frames would not result in very large strain energy [23]. If $f_1(r)$, $f_2(r)$, . . . $f_T(r)$ and $m_1(r)$, $m_2(r)$, . . . $m_T(r)$ were denoted T frames image and T motion fields between each successive two frames respectively, the important non-negative condition on each intensity function f_t will be denoted by $f \geq 0$ [17]. Then the negative log likelihood term of an objective function was defined as Equation (2-2) [17]:

$$L(f) = \sum_{t=1}^{T} \sum_{i=1}^{M} \left[Hf_t(i) - g^{(t)}(i) \log Hf_t(i) \right], \qquad (2\text{-}2)$$

where M was the total number of the detector bins, the dimension of the phantom, H was the projection operator, and $g_1(t)$, $g_2(t)$, . . . $g_T(t)$ were gated datasets.

2.4.2.2 Image matching term

When the image intensities between frames t and t + 1 perfectly matched the motion field m_i between them, $f_t(r)$ should equal to $f_{t+1}(r+m_t(r))$ for all r [17]. In practice, image frames and motion fields were never exactly matched. Therefore, the image matching term of an objective function between frames t and t + 1, which defined as Equation (2-3) [17], was expected to be small:

$$E_I(f_t, f_{t+1}; m_t) = \int \left[f_t(r) - f_{t+1}(r + m_t(r)) \right]^2 dr , \qquad (2\text{-}3)$$

where r was the voxel coordinate, and r = (x, y, z). If considered the entire cardiac cycle, the total image matching term was defined as Equation (2-4) [17]:

$$\varepsilon_I(f; m) = \sum_{t=1}^{T} E_I(f_t, f_{t+1}; m_t). \qquad (2\text{-}4)$$

2.4.2.3 Strain energy term

By treated myocardium as a deformable elastic material, material strain resulting from the cardiac motion can be modeled by the strain energy [17]. The strain energy depended on the derivatives of the motion vector and material parameters λ and μ, namely Lamè Constants [15]. After several experiments, it was found that the material difference can be ignored in this study. Next, λ and μ were set equal to one both inside and outside the myocardium so that Young's modulus was $\mu(3\lambda + 2\mu)/(\lambda + \mu) = 2.5$ and Poisson's ratio was $0.5\ \lambda/(\lambda + \mu) = 0.25$ respectively In this study. Segmentation process by Mair *et al.* [17] was still included in this work, but only applied for evaluation method for image quality and motion accuracy presented in Chapter 3. For each motion field between frame t and t + 1, m_t had three components u_t, v_t, and w_t. By applying the strain energy function in Love's classical book [15], the strain energy term of an objective function was defined as Equation (2-5) [17]:

$$\begin{aligned} &\varepsilon_S(m) = \sum_{t=1}^{T} E_S(m_t), \text{where} \\ &E_S = \frac{1}{2}\int \lambda(r)\left(u_{t,x} + v_{t,y} + w_{t,z}\right)^2 dr + \int \mu(r)\left(u_{t,x}^2 + v_{t,y}^2 + w_{t,z}^2\right)dr \\ &\quad + \frac{1}{2}\int \mu(r)\left[\left(u_{t,y} + v_{t,x}\right)^2 + \left(u_{t,z} + w_{t,x}\right)^2 + \left(v_{t,z} + w_{t,y}\right)^2\right]dr, \end{aligned} \tag{2-5}$$

where $u_{t,x}$, $v_{t,y}$, $w_{t,x}$, . . . were continuous first partials. e.g. $u_{t,x} = \frac{\partial u_t}{\partial x}$. λ and μ were included here for general expression. They were assigned to ones in this study. Finally, the total objective function was defined as Equation (2-6) [17]:

$$\varepsilon(f; m) = \alpha L(f) + E_I(f; m) + \beta\varepsilon_S(m), \tag{2-6}$$

where α and β were hyper-parameters, which reflected the influence that image matching, projection data and strain energy have on the estimations. Upon several experiments by Mair *et al.* [17], the value of α and β were determined as 0.015 and 0.0035 respectively in this study.

If $f_1^*(r), f_2^*(r), \ldots f_T^*(r)$ and $m_1^*(r), m_2^*(r), \ldots m_T^*(r)$ were denoted true images and true motion fields respectively, minimized function ε resulted as Equation (2-7) [17]:

$$(f^*; m^*) = \arg\min_{f \geq 0, m} \varepsilon(f; m) . \quad (2\text{-}7)$$

In RM algorithm, the initials were uniformed images and zero motion fields. The reconstructed images were updated first while motion fields were fixed (R Step). Then the estimated cardiac wall motions were updated while image frames were fixed (M Step). Within R Step or M Step, the algorithm went out of loop when it was converged. After one R Step and one M Step, each image and motion field was updated once equally. In R step, image matching and negative log likelihood terms of the objective function were used to improve the reconstructed images. The expected estimate for each iterative R step was defined as Equation (2-8) [17]:

$$f^{n+1} = \arg\min_{f \geq 0} \varepsilon(f; m^{(n)}) . \quad (2\text{-}8)$$

In M step, updated frames in latest R step were used to improve estimated motions. The expected estimate for each iterative M step was defined as Equation (2-9) [17]:

$$m^{n+1} = \arg\min_{m} \varepsilon(f^{(n+1)}; m) . \quad (2\text{-}9)$$

Experimental results of the reconstructed images and estimated cardiac wall motions are presented in Chapter 3.

2.4.3 Reconstruction and Motion Estimation

100-iteration RM algorithm, with 100-iteration R step and 100-iteration M alternately, was applied to all projection datasets *ORMA*, *ORMU*, and *ORMC*. Fortran code was running on Penguin Tempest 2100 (Dual-processor 64-bit AMD Opteron, 8 GB physical memory). It took about 4 hours to finish 100 iterations. The value of α and β were assigned as 0.015 and 0.0035 respectively according to Mair *et al.* [17].

2.5 Image Quality and Cardiac Wall Motion Accuracy Evaluation Methods

The image quality of the reconstructed image was evaluated using Sum of Squared Errors (SSE) method. The accuracy of the cardiac wall motion estimation was evaluated using images matching term of the objective function. For the evaluation, phantom *OHM* was using as the reference, and the image matching equation was also named Phantom-matching Motion Error (PME) method.

2.5.1 Image Quality Evaluation

For image quality evaluation, SSE method was defined as Equation (2-10) [17]:

$$SSE(f,\hat{f}) = \sum_{t=1}^{T}\sum_{r}\left(f_t(r) - \hat{f}_t(r)\right)^2, \qquad (2\text{-}10)$$

where $f_1(r), f_2(r),... f_T(r)$ and $\hat{f}_1(r), \hat{f}_2(r),... \hat{f}_T(r)$ were phantom source distributed object and reconstructed image, respectively. Only the voxels inside the myocardial region would be summed. A segmentation map was generated to define the moycardium by given a threshold intensity. In this study, only heart was included in the phantom. Therefore, the intensity threshold was assigned as zero. In another word, any non-zero intensity voxel was considered within myocardium. The segmentation map and the

experimental results were shown in Chapter 3. SSE evaluation method was also used for α value optimization study [17].

2.5.2 Cardiac Wall Motion Evaluation

Recall image matching equation:

$$E_I(f_t, f_{t+1}; m_t) = \int \left[f_t(r) - f_{t+1}(r + m_t(r)) \right]^2 dr \,. \qquad (2\text{-}3)$$

For cardiac wall motion evaluation, same equation was used but called PME method defined as Equation (2-11) [17]:

$$PME(\hat{m}) = \sum_{t=1}^{T} \sum_{r} \left(f_t(r) - f_{t+1}(r + \hat{m}_t(r)) \right)^2 , \qquad (2\text{-}11)$$

where $f_t(r)$ was the phantom source distributed object at frame t, and $\hat{m}_t(r)$ was the estimated motion field from frame t to frame t + 1. If frame t is the last frame in a sequence (e.g. the 8th frame in a 8-gate cardiac image cycle), frame t + 1 would be assigned to be the first frame in the cycle. In this evaluation study, only those non-zero intensity voxels were considered within myocardium and were computed for PME value. The segmentation map was used, too. The experimental results were shown in Chapter 3. PME evaluation method was used for β value optimization study, too [17].

CHAPTER 3
EXPERIMENTAL RESULTS AND DISCUSSION

3.1 Simulated Phantoms, True Motion Field, and Projections

Experimental results and analysis are presented in this Chapter. Calculated relative center-of-mass of projections before and after respiratory compensation, reconstructed images, estimated cardiac wall motion, and SSE and PME evaluation data are illustrated in the following sections.

3.1.1 Cardiac Gated NCAT Phantom

3.1.1.1 Reference phantom with beating heart motion only

As a reference phantom, eight cardiac beating frames are shown in figure 3-1 in trans-axial and coronal orientations of a phantom with beating heart motion only. The dimension of the phantom was $96 \times 96 \times 50$ for each gating frame. End-diastole and end-systole can be seen clearly at frame 1 and frame 4, respectively.

3.1.1.2 Phantom with both beating heart motion and respiratory motion

To look at whether respiratory motion had an effect on myocardial imaging, a phantom with combined beating heart motion and respiratory motion is shown in Figure 3-2. If the length of the respiratory cycle was assigned as 5 seconds, and the length of the beating heart cycle was assigned as 1 second, there were 5 complete beating heart cycles during one respiratory cycle. The first beating heart frame for each one of the five beating heart cycles at different respiratory phases are displayed in Figure 3-2. Myocardium shifted down about 2 centimeters from full exhalation to full inhalation with the diaphragm.

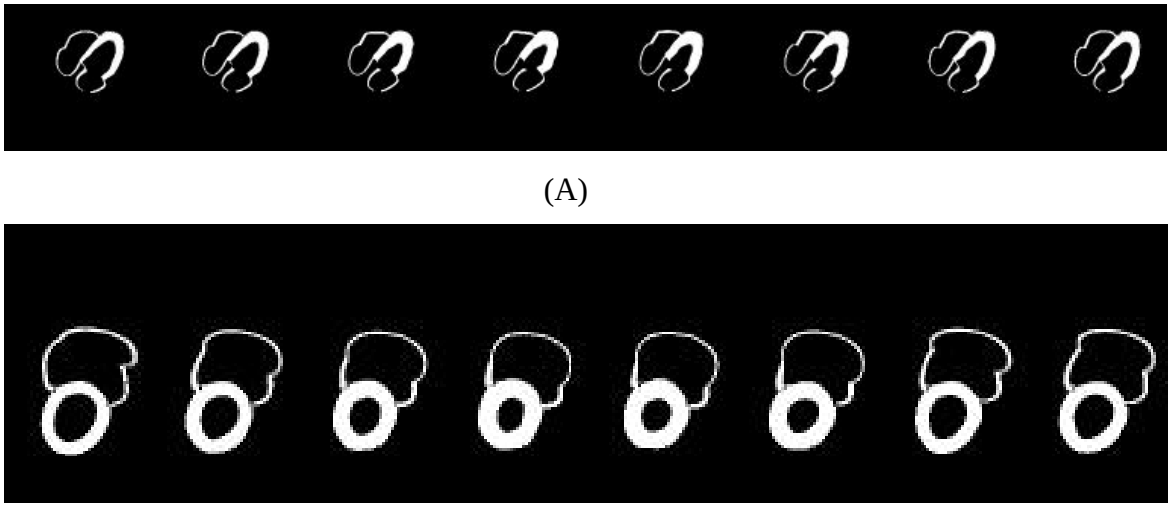

(A)

(B)

Figure 3-1. Eight cardiac beating frames of a NCAT phantom with beating heart motion only. (A) Frame 1 to 8 on trans-axial orientation. (B) Frame 1 to 8 on coronal orientation.

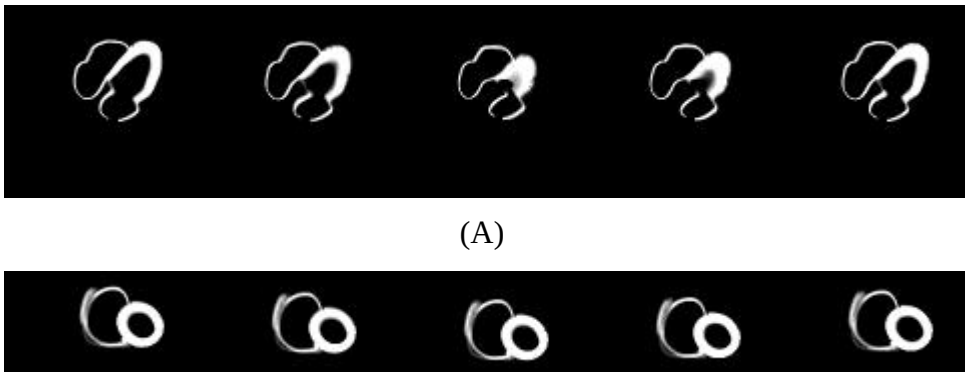

(A)

(B)

Figure 3-2. Beating heart frame 1 at different respiratory phases. (A) Trans-axial orientation. (B) Coronal orientation.

3.1.2 True Motion Field of the NCAT Phantom

The true motion field for the beating heart motion only phantom was superimposed on the reference object and is plotted in Figure 3-3. Frames in the left column showed the end-diastole. All motion vectors were pointing to the direction where the heart contracted to during systole. Frames in the right column show the end-systole. All motion vectors point to the direction where the heart enlarged to during diastole.

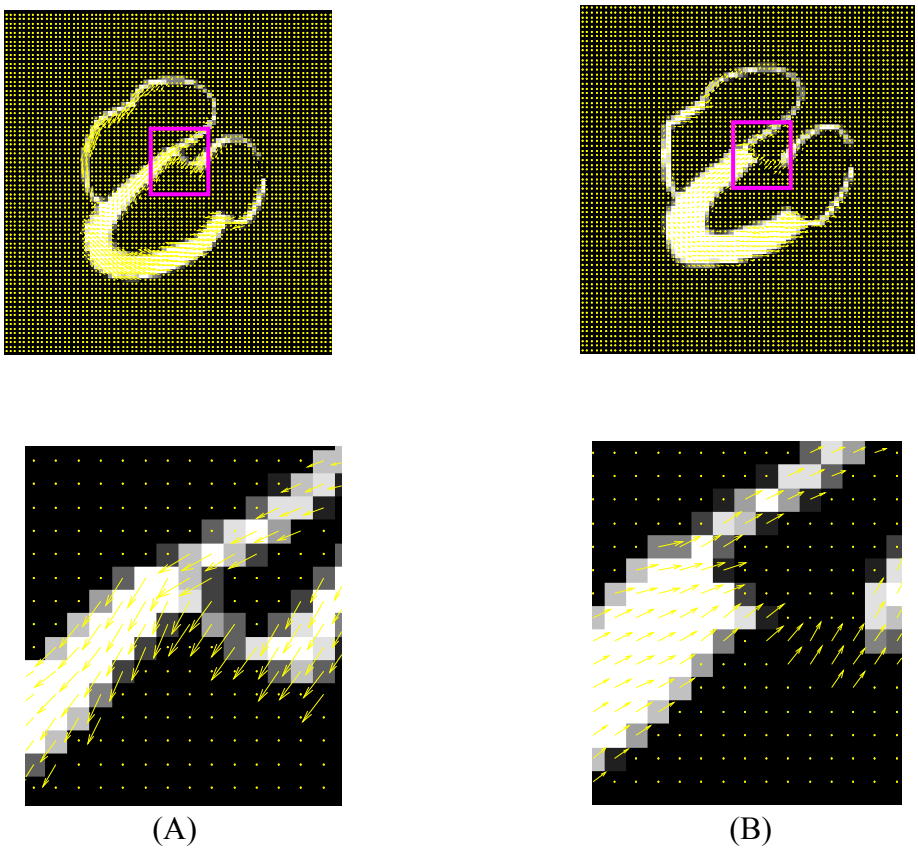

(A) (B)

Figure 3-3. True Beating Heart Motion generated by NCAT software.
Column (A): end-diastole; Column (B): end-systole.

3.1.3 Projection Datasets

Projection dataset *OHM* is shown in Figure 3-4. Dataset *ORMA* is shown in Figure 3-5. Only projection angle 38 of each dataset is shown in these two figures. It was observed that cardiac gated projection data were blurred by the respiratory motion obviously. Hence, the respiratory motion effect could not be ignored during the SPECT imaging. Figure 3-6 and Figure 3-7 show the first frame for each beating heart cycle over respiratory phases (5 phases shown in this example). Projection data angle 1, 38 and 60 are shown in these two figures. Linear axial movement can be seen vertically from Figure 3-6. Purple line indicates the heart position without respiratory effect. No trans-

axial movement horizontally is found as expected how the phantom been modeled from Figure 3-7.

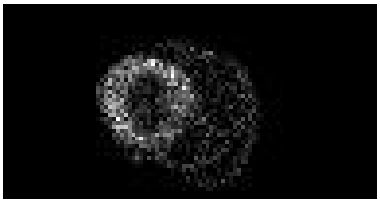

Figure 3-4. Projection data simulated from OHM.

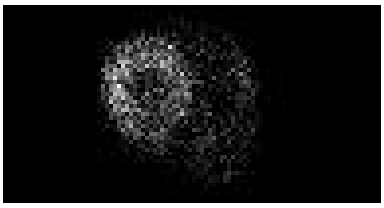

Figure 3-5. Projection data simulated from ORMA.

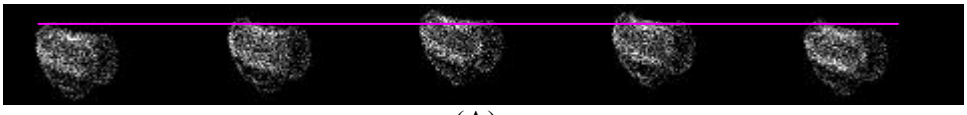

(A)

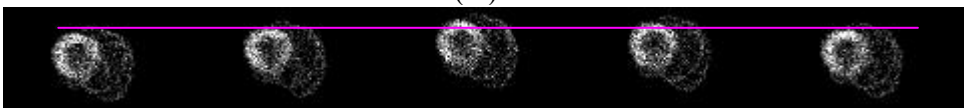

(B)

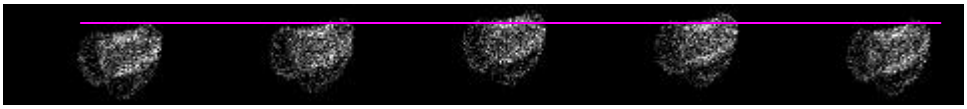

(C)

Figure 3-6. Projection dataset ORMU showing linear axial movement of the heart due to respiratory motion in different angles.
(A) Projection angle 1, (B) Projection angle 38, (C) Projection angle 60.

3.2 aCOM Calculation and Respiratory Motion Compensation Method

The relative COM along axial direction of projection datasets *ORMU* and *ORMC* were presented in the following sections. The COM of each respiratory phase over the cycle was also shown here.

3.2.1 aCOM Calculation

Figure 3-8 illustrated the relative COM of projection dataset *ORMU* along axial

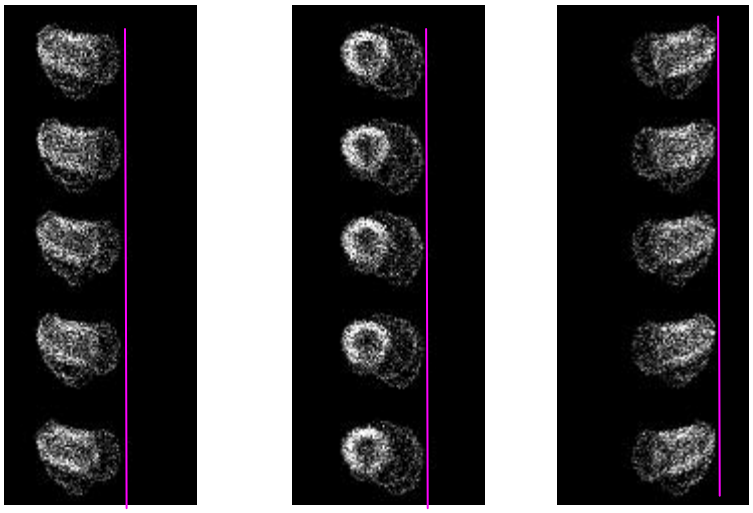

(A) (B) (C)

Figure 3-7. Projection dataset ORMU showing no trans-axial movement of the heart due to respiratory motion in different angles.
(A) Projection angle 1, (B) Projection angle 38, (C) Projection angle 60.

direction calculated by using Equation (2-1) for each cardiac frame over one entire respiratory cycle. Compare to the 2-centimeter linear translation due to the respiratory motion, the magnitude of the movement due to the heart beating (average about 0.15 centimeters) was unobservable. Therefore, only the displacement caused by the respiratory motion could be seen from the chart.

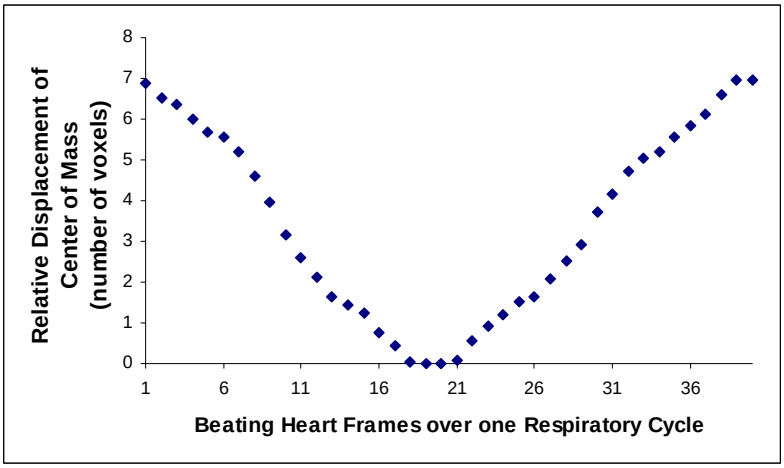

Figure 3-8. The relative center of mass for each beating heart frame over one respiratory cycle

3.2.2 Respiratory Motion Compensation

Five phases (gates) over one 5-second entire respire cycle was calculated first because of the simplicity. Ten phases and twenty phases respiratory schema were also simulated for comparison and optimization. All three gate schema were shown in Figure 3-9. The height of each column indicates how much the beating heart frames within that respiratory phase need to be shifted.

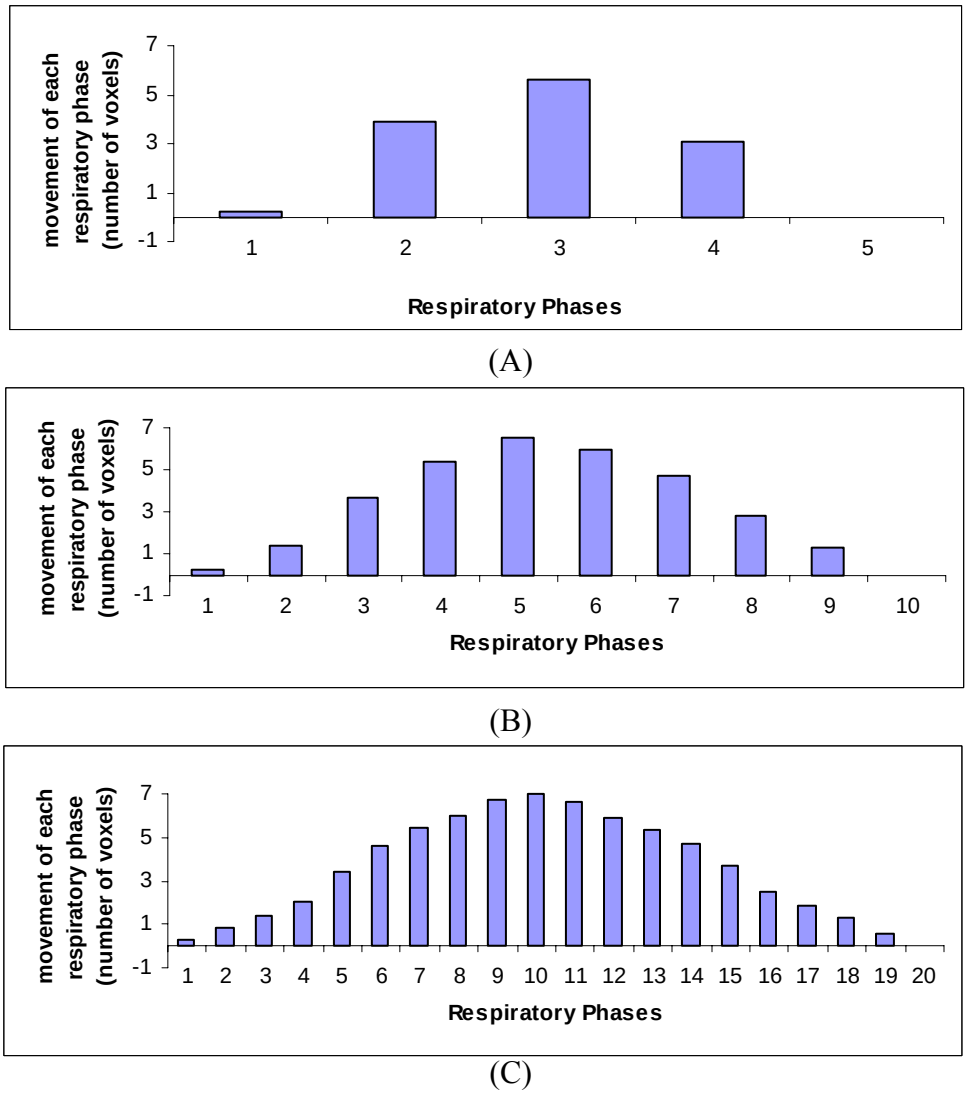

Figure 3-9. Measured movement due to respiratory motion of each respiratory phase for different gate (phase) schema for a 5-second entire respiratory cycle. (A) 5 Phases. (B) 10 Phases. (C) 20 Phases.

After respiratory motion compensation, the relative COM for each beating heart frame should be very close to the reference phase. The ideal illustration should be a straight horizontal line. The error depends on which gate schema was used. The more gates used for each respiratory cycle, the less errors were. Twenty phases schema would be chosen according to the clinical realization by Cho *et al.* [10]. The projection datasets of projection angle 38 after (*ORMC*) 20-phase respiratory motion correction is shown in Figure 3-10. Respiratory motion blurred projection data (*ORMA*) and heart motion only projections (*OHM*) were shown in the same figure for comparison. The projection data can be seen from the images clearly that it was very close to the reference projections (*OHM*) after motion compensation. In practice, the respiratory motion might not be very stable. The length of the respiratory cycle might change during projection data acquisition. Over sampling of the gates and averaging over each chosen respiratory phase would contribute to the motion compensation improvements.

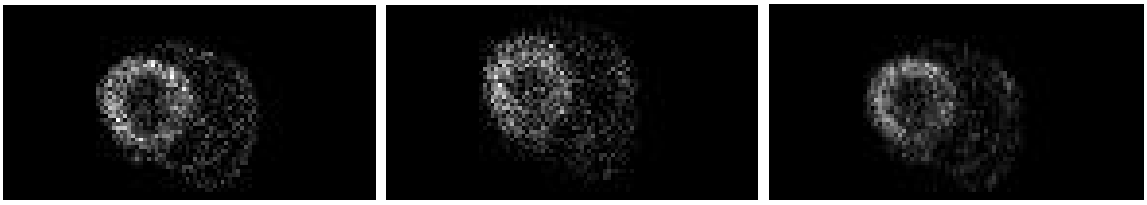

(A) (B) (C)

Figure 3-10. Projection datasets OHM, ORMA, and ORMC.
(A) OHM. (B) ORMA. (C) ORMC.

3.3 Image Reconstruction, Cardiac Wall Motion Estimation, and SSE and PME Evaluations.

The RM reconstructed images from all three projection datasets (*OHM*, *ORMA*, and *ORMC*) are shown in this section. SSE and PME evaluations are listed in the tables here.

3.3.1 Image Reconstruction and Wall Motion Estimation

The reconstructed images and profile plots from all three projections (*OHM*, *ORMA*, and *ORMC*) for three orthogonal slice orientations trans-axial, coronal, and sagittal are shown in Figure 3-11, Figure 3-12 and Figure 3-13, respectively. 20 respiratory phases schema were chosen to show result in this study according to the clinical level determined by Cho *et al.* [10].

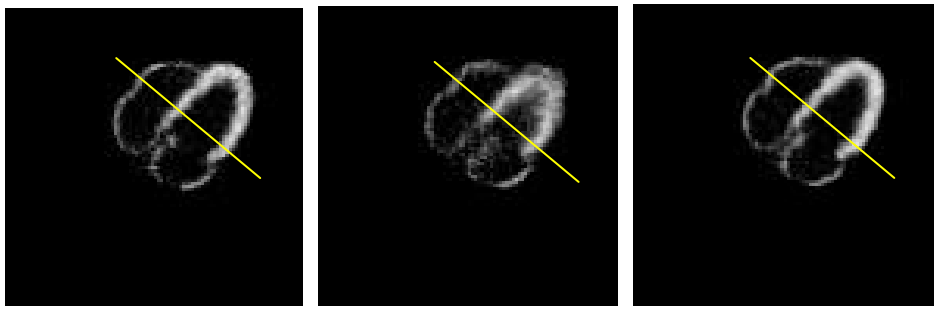

(A) (B) (C)

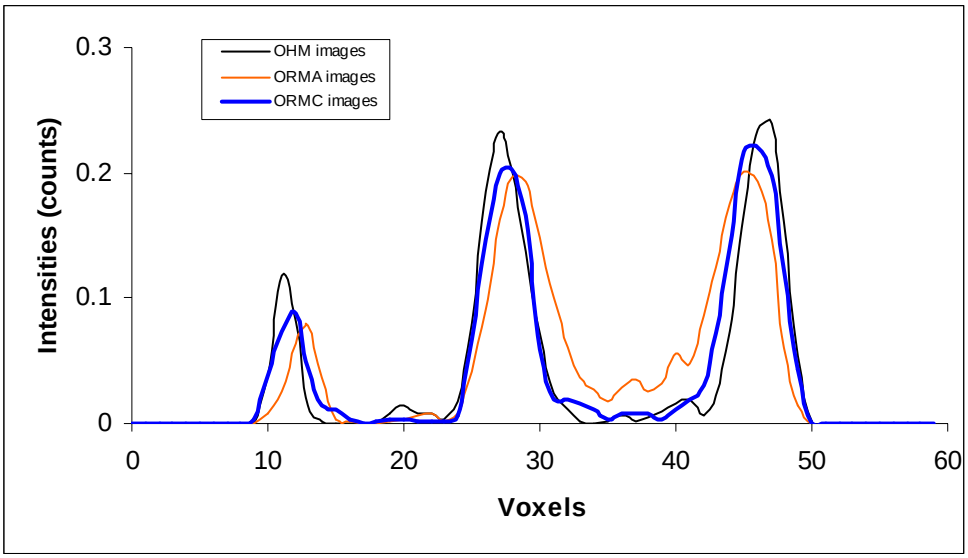

(D)

Figure 3-11. Reconstructed images by RM algorithm and profile plot from projection datasets OHM, ORMA, and ORMC. (trans-axial orientation)
(A) OHM. (B) ORMA. (C) ORMC. (D) Profiles

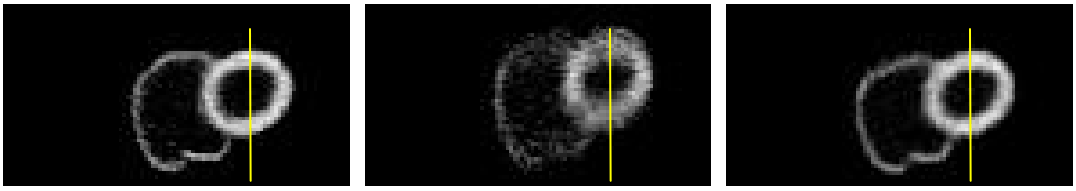

(A) (B) (C)

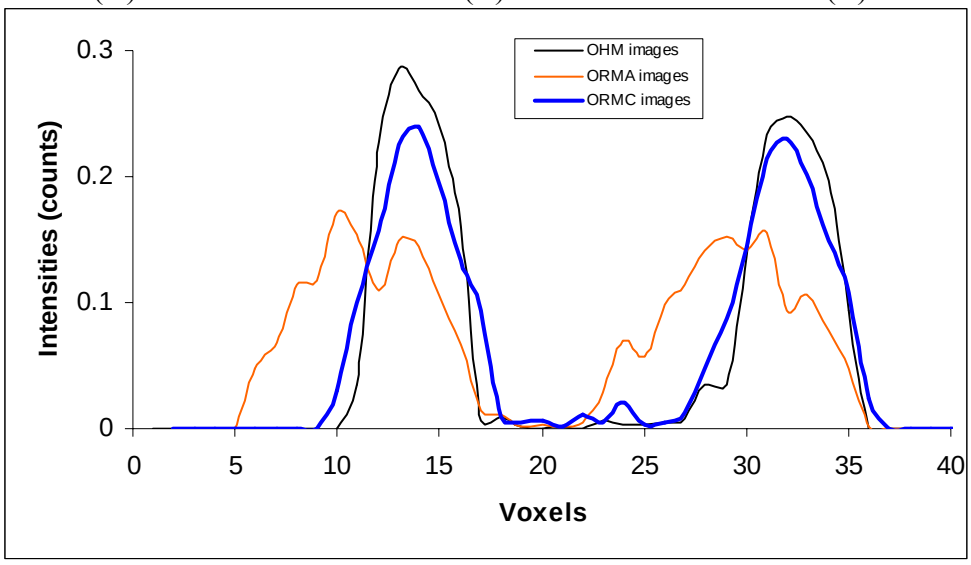

(D)

Figure 3-12. Reconstructed images by RM algorithm and profile plot from projection datasets OHM, ORMA, and ORMC. (coronal orientation)
(A) OHM. (B) ORMA. (C) ORMC. (D) Profiles

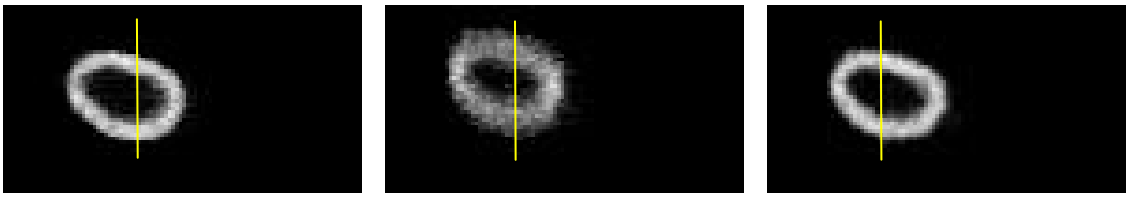

(A) (B) (C)

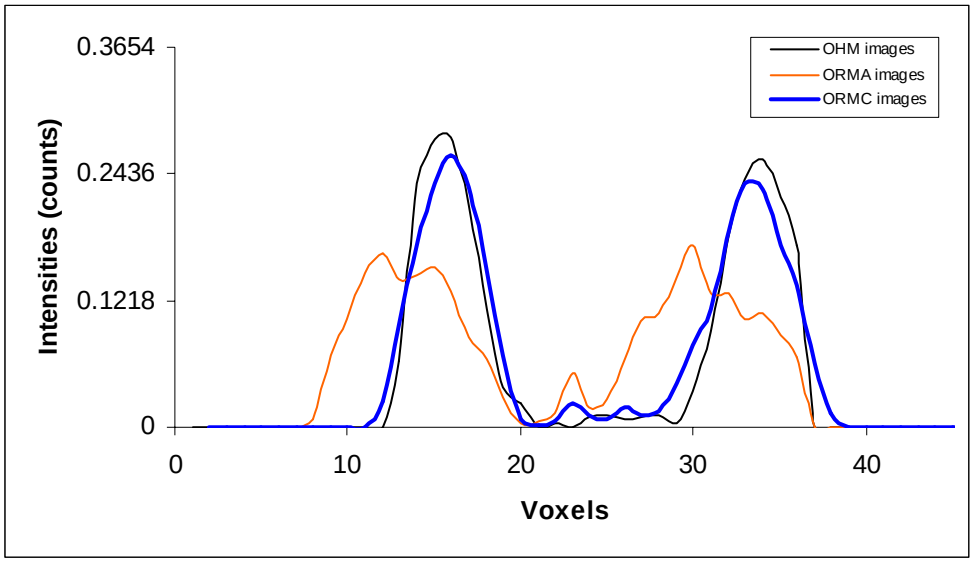

(D)

Figure 3-13. Reconstructed images by RM algorithm and profile plot from projection datasets OHM, ORMA, and ORMC. (sagittal orientation)
(A) OHM. (B) ORMA. (C) ORMC. (D) Profiles

From the reconstructed images in all orientations, it was observed that the blurring due to the respiratory motion had been reduced greatly by motion compensation method. The image reconstructed from corrected projections was much closer to the image reconstructed from the reference dataset. *ORMC* images looked smoother than true (*OHM*) images. That was because *ORMC* images were summed over respiratory phases after motion compensation. From the profile plots, it was observed that both *OHM* images and *ORMC* images peak were narrow and had higher peak values. It demonstrated that the noise control was improved, and the less blurring on the edge of the

myocardial region could be seen, too. Estimated wall motion would be evaluated by PME method explained in next section.

3.3.2 SSE and PME Evaluation Method

The segmentation map used for SSE and PME evaluation study is shown in Figure 3-14. Slice 27 in frame 1 was chosen to show here.

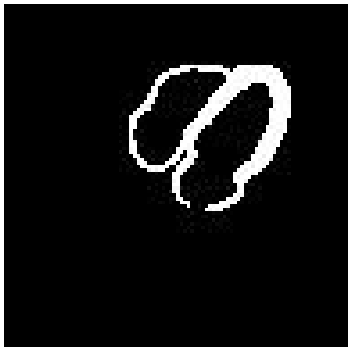

Figure 3-14. Segmentation map of myocardial region for image quality and motion estimation accuracy evaluation

The SSE evaluation results of *OHM*, *ORMA*, and *ORMC* images calculated by Equation (2-10) are listed in Table 3-1. The PME evaluation results of *OHM*, *ORMA*, and *ORMC* motion fields calculated by Equation (2-11) are listed in Table 3-2. The SSEs and PMEs values as a function of number of respiratory phases are shown in Figure 3-15.

Table 3-1. The SSE results of OHM, ORMA, and ORMC images quality evaluation.

	Sum of Squared Errors (SSE)
True Object	0
OHM image	472.48
ORMA image	1503.93
ORMC image (5 phases)	643.57
ORMC image (10 phases)	560.54
ORMC image (20 phases)	521.79

Table 3-2. The PME results of OHM, ORMA, and ORMC motion estimation accuracy evaluation.

	Phantom-matching Motion Errors (PME)
True motion	88.25
OHM motion	183.75
ORMA motion	386.35
ORMC motion (5 phases)	307.37
ORMC motion (10 phases)	290.85
ORMC motion (20 phases)	272.91

From the SSEs and PMEs table, respiratory motion compensation method demonstrated improved SSE error as well as improved image noise and spatial resolution characteristics. Both SSE and PME would decrease with the increased number of respiratory phases. Also according to the clinical study by Cho *et al.* [10], 20 phases would be an ideal choice for respiratory-gated study.

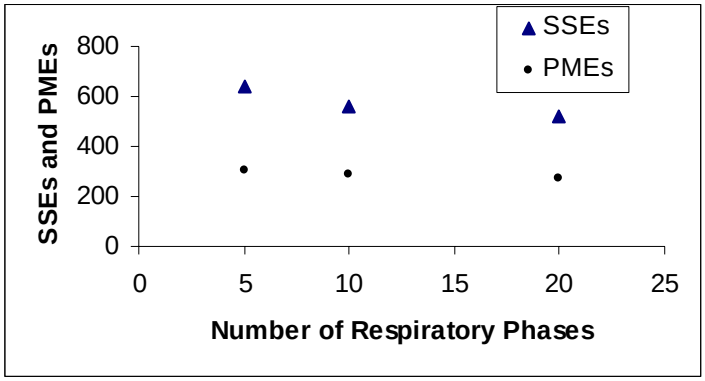

Figure 3-15. SSEs and PMEs as a function of number of respiratory phases.

CHAPTER 4
CONCLUSIONS AND FUTURE WORK

4.1 Summary and Conclusions

A respiratory motion compensation method was discussed and developed in this study. Method was implemented by a NCAT phantom simulation with both beating heart motion and respiratory motion. Respiratory motion was tracked and estimated by aCOM algorithm. Motion compensation was realized by applying method on to the projections computed from the NACT phantoms with a linear interpolation operator. The true projection, averaged projection and the corrected projection datasets were reconstructed by RM algorithm. The cardiac wall motion was estimated simultaneously with the image reconstruction. The respiratory motion compensation method was evaluated by comparison between *OHM*, *ORMA* and *ORMC* images and motion fields. Numerical results were explained by calculation of SSEs and PMEs errors.

- From the projections, it was observed that cardiac gated projection data were blurred by the respiratory motion.
- From aCOM calculation, the respiratory motion can be tracked and estimated for each respiratory phase.
- After respiratory motion compensation by aCOM computations, the corrected projection data are very close to the data without respiratory motions.
- It can be seen that blurring are reduced on the reconstructed images from the corrected projection data. From the evaluation results, the values of SSE and PME demonstrated improved spatial resolution and more accuracy of wall motion estimation than that without respiratory motion compensation.
- Different respiratory phases' schemas have been tested. More respiratory gating sampling gives more image quality improvement and more accuracy on wall

motion estimation. According to the clinical patient data study of other papers, 20 respiratory phases are chosen for this study.

4.2 Future Work

The study included only the heart for the NCAT phantom simulation. Since for gated myocardial perfusion SPECT imaging with Tc-99m, the radiopharmaceuticals will generate intensities in the other organs, such as liver, almost same level relative to the heart. That may have big effect on the center-of-mass calculation to track and estimated the respiratory motion. Future studies using phantoms with more organs can make this compensation method more general.

In this study, it was assumed that the respiratory motion was constant within one respiratory phase. In practice, the respiratory gate can not be too narrow. This will bring errors to the simulation with both beating heart and respiratory motion, because within one respiratory phase (e.g. less than 5-phase schema), there are more than one beating heart frames included. One beating heart frame was the time bin which was finally implemented. Further consideration of more cardiac cycle and respiratory cycle combination may yield more accurate results. Respiratory motion effect will take place in almost every myocardial perfusion SPECT imaging examination. In practice, the respiratory cycle may not be fixed during imaging, and the beating heart motion and respiratory motion combination could be more complicated. Applying this compensation method to clinical patient data would be an important future study.

LIST OF REFERENCES

1. Gottschalk A, Harper PV, Jimenez FF, Petasnick JP. Quantification of the respiratory scanning with the rectilinear focused collimator scanner and the gamma scintillation camera. *Journal of Nuclear Medicine.* 1966;7:243–251.

2. Zubal G, Bizais Y, Bennett GW, Brill AB. Dual gated nuclear cardiac images. *IEEE Transactions on Nuclear Science.* 1984;31:566–569.

3. Klein GJ, Reutter BW, Ho MH, Reed JH, Huesman RH. Real-time system for respiratory-cardiac gating in positron tomography. *IEEE Transactions on Nuclear Science*. 1998;45(4):2139–2143.

4. Klein GJ, Reutter BW, Huesman RH. Data-driven respiratory gating in list mode cardiac PET. *Journal of Nuclear Medicine.* 1999;40(5):113P.

5. Oppenheim BE. A method using a digital compute for reducing respiratory artifacts on liver scans made with a camera. *Journal of Nuclear Medicine.* 1971;12:625–628.

6. Schmidlin P. Development and comparison of computer methods for organ motion correction in scintigraphy. *Journal of Nuclear Medicine.* 1999;40(5):113P.

7. Hoffer PB, Oppenheim BE, Stterling ML, Yasillo N. A simple device for reducing motion artifacts in gamma camera images. *Radiology*. 1972;103:199–120.

8. Baimel NH, Bronskill MJ. Optimization of analog-circuit motion correction for liver scintigraphy. *Journal of Nuclear Medicine.* 1978;19:1059–1066.

9. Wang Y, Riederer SJ, Ehman RL. Respiratory motion of the heart: kinematics and the implications for the spatial resolution in coronary imaging. *Magnetic Resonance in Medicine.* 1995;33:713–719.

10. Cho K, Kumiata S, Okada S, Kumazaki T. Development of respiratory gated myocardial SPECT system. *Journal of Nuclear Cardiology.* 1999;6:20–28.

11. Segars WP, Lalush DS, Tsui BMW. Modeling respiratory mechanics in the MCAT and spline-based MCAT phantoms. *IEEE Transactions on Nuclear Science.* 2001;48(1):89–97.

12. Segars WP, Tsui BMW. Study of the Efficacy of Respiratory Gating in Myocardial SPECT Using the New 4-D NCAT Phantom. *IEEE Transactions on Nuclear Science.* 2002;49(3):675–679.

13. Feng B, Bruyant PP, Pretorius PH, Beach RD, Gifford HC, Dey J, Gennert M, King MA. Estimation of the rigid-body motion from three-dimensional images using a generalized center-of-mass points approach. *IEEE Nuclear Science Symposium Conference Record.* 2005;M07:248.

14. Bruyant PP, King MA, Pretorius PH. Correction of the respiratory motion of the heart by tracking of the center of mass of thresholded projections: a simulation study using the dynamic MCAT phantom. *IEEE Transactions on Nuclear Science*. 2002;49(5):2159–2166.

15. Segars WP. Development of a new dynamic NURBS-based cardiac torso (NCAT) phantom. *Ph.D. dissertation*. The University of North Carolina, Chapel Hill, 2001.

16. Cao Z, Simultaneous reconstruction and 4D motion estimation for gated myocardial emission tomography. *Ph.D. dissertation*. The University of Florida, Gainesville, 2003.

17. Mair BA, Gilland DR, Sun J, Estimation of images and non-rigid deformations in gated emission CT. *Transactions on Medical Imaging.* Accepted in April, 2006.

18. Narayanan MV, King MA, Soares EJ, Byrne CL, Pretorius PH, Wernick MN. Application of the Karhunen-Loeve transform to 4D reconstruction of cardiac gated SPECT images. *IEEE Transactions on Nuclear Science*. 1999;46(4):1001–1008.

19. Mair BA, Gilland DR, Cao Z. Simultaneous motion estimation and image reconstruction from gated data. *IEEE International Symposium on Biomedical Imaging*, 2002:661–664.

20. Cao Z, Gilland DR, Mair BA, Jaszczak RJ. Three-dimensional motion estimation with image reconstruction for gated cardiac ECT. *IEEE Transactions on Nuclear Science.* 2003;50(3):384–388.

21. Gilland DR, Mair BA, Sun J. Joint 4D reconstruction and motion estimation in gated cardiac ECT. *Intern Conference on Fully 3D Image Reconstruction Radiation Nuclear Medicine.* 2005:303.

22. Klein J, Reutter BW, Huesman RH. Non–rigid summing of gated PET via optical flow. *IEEE Transactions on Nuclear Science*. 1997;44(4):1509–1512.

23. Klein GJ, Huesman RH. Elastic material model mismatch effects in deformablemotion estimation. *IEEE Transactions on Nuclear Science*. 2000;47(3):1000–1005.

24. Love AEH, A Treatise on the Mathematical Theory of Elasticity. Dover Publications. New York, 1944.

25. Humphrey JD, Delange SL. An introduction to biomechanics: solids and fluids, analysis and design. Springer-Verlag. New York, 2004.

BIOGRAPHICAL SKETCH

Jing Sun was born in Jilin, China, on February 28th, 1976. In September 1994, she began her college education in Tsinghua University in Beijing and obtained her Bachelor of Science degree in engineering physics in July 1999. In 2002, she obtained her Master of Science degree in nuclear engineering from North Carolina State University.

In August 2003, Jing was admitted to the University of Florida as a graduate student to the medical physics program in the Department of Nuclear and Radiological Engineering. During the last three years, she has worked with Dr. David Gilland in SPECT myocardial imaging project.

Jing Sun is the only daughter of Zhongzhi Sun and Guirong Liu and is married to Dapeng Ding.